frontiers in Chemistry

ORIGINAL RESEARCH
published: 15 April 2021
doi: 10.3389/fchem.2021.667878

# Macroscale Superlubricity Accomplished by $Sb_2O_3$-MSH/C Under High Temperature

*Kai Gao*[1,2], *Bin Wang*[1], *Asghar Shirani*[3], *Qiuying Chang*[2] *and Diana Berman*[3]*

[1] State Key Laboratory of Tribology, Tsinghua University, Beijing, China, [2] School of Mechanical, Electronic and Control Engineering, Beijing Jiaotong University, Beijing, China, [3] Materials Science and Engineering Department, University of North Texas, Denton, TX, United States

Here, we report the high-temperature superlubricity phenomenon accomplished in coatings produced by burnishing powders of antimony trioxide ($Sb_2O_3$) and magnesium silicate hydroxide coated with carbon (MSH/C) onto the nickel superalloy substrate. The tribological analysis performed in an open-air experimental setup revealed that with the increase of testing temperature, the coefficient of friction (COF) of the coating gradually decreases, finally reaching the superlubricity regime (the COF of 0.008) at 300°C. The analysis of worn surfaces using *in-situ* Raman spectroscopy suggested the synergistic effect of the inner $Sb_2O_3$ adhesion layer and the top MSH/C layer, which do not only isolate the substrate from the direct exposure to sliding but also protect it from oxidation. The cross-sectional transmission electron microscopy (TEM) and X-ray photoelectron spectroscopy (XPS) results indicated the tribochemically-activated formation of an amorphous carbon layer on the surface of the coating during sliding. Formation of the film enables the high-temperature macroscale superlubricity behavior of the material system.

**Keywords: macroscale superlubricity, magnesium silicate hydroxide, $Sb_2O_3$, burnishing, high-temperature, tribology, tribochemistry**

OPEN ACCESS

***Edited by:***
*Seong H. Kim,*
*Pennsylvania State University (PSU), United States*

***Reviewed by:***
*Wei Zhang,*
*Jilin University, China*
*Qianzhi Wang,*
*Nanjing University of Aeronautics and Astronautics, China*

***Correspondence:**
*Diana Berman*
*diana.berman@unt.edu*

***Specialty section:***
*This article was submitted to Physical Chemistry and Chemical Physics, a section of the journal Frontiers in Chemistry*

***Received:*** *15 February 2021*
***Accepted:*** *23 March 2021*
***Published:*** *15 April 2021*

***Citation:***
*Gao K, Wang B, Shirani A, Chang Q and Berman D (2021) Macroscale Superlubricity Accomplished by $Sb_2O_3$-MSH/C Under High Temperature. Front. Chem. 9:667878. doi: 10.3389/fchem.2021.667878*

## INTRODUCTION

Superlubricity [the coefficient of friction (COF) is <0.01], or the sliding regime with friction approaching almost zero values, is one of the research hotspots in the tribology field (Berman et al., 2018a). It was first proposed by Motohisa Hirano (Hirano and Shinjo, 1993) to describe a theoretical state: the friction force is extremely small or vanished between the tribopairs. So far, the superlubricity was mostly demonstrated for the laboratory-scale experiments, while use of the superlubricity in the large-scale industrial set-ups remains challenging. Previous studies demonstrated superlubricity mostly with 2D materials (Berman et al., 2018a), including graphite (Dienwiebel et al., 2004; Liu et al., 2012), graphene (Berman et al., 2015, 2019; Kawai et al., 2016), molybdenum disulfide ($MoS_2$) (Martin et al., 1993; Li et al., 2017; Berman et al., 2018b), boron nitride (BN) (Zeng et al., 2013), black phosphorus (BP) (Wang et al., 2018a,b). The mechanism of the superblurcitiy that uses the easy shearing properties of 2D materials is also called structural superlubricity. In addition to two-dimensional materials, there are other ways to achieve superlubricity. For example, Li et al. (2014) tried to mix acids with glycerol or polyhydroxy alcohols that contained large amounts of hydroxyl groups indicating that the possible superlubricity mechanism was associated with the formation of a fluid-hydrated water layer between glycerol and water or polyhydroxy alcohol and water on the positively charged surfaces.

Meanwhile, most of the previous studies demonstrating superlubricity regime with solid lubricants focused on material systems that work at room temperature conditions. As a result, the justified cases of the superlubricity became very limited in terms of their applications. In efforts to solve the tribological challenges related to high temperature applications, focus was rather directed toward ternary oxides and carbides that are in general incapable of near-zero friction sliding (Gao et al., 2015; Aouadi et al., 2020). A possible solution is to enable adaptive behavior of materials under changes in the testing conditions which was successfully shown in case of graphite-$MoS_2$ chameleon coatings (Shirani et al., 2020). The COF values were significantly reduced (down to 0.02 values) when testing the materials at elevated temperature conditions.

Here, we demonstrate that the superlubricity regime can be achieved at elevated temperature conditions in an open-air system by activating the formation of the low-friction tribofilm during sliding when using magnesium silicate hydroxide coated with a carbon layer (MSH/C). Magnesium silicate hydroxide is a novel lubricant additive and the main component of serpentine mineral with its tribological properties mainly being dependent on the release of Si-O, Mg-O, and -OH active groups that form a tribochemical layer during the friction process (Yu et al., 2010, 2013). To improve adhesion of the MSH/C film to the substrate material, we used antimony oxide ($Sb_2O_3$) powders (melting point: 656°C, boiling point: 1,425°C) (Jha et al., 2009). Though $Sb_2O_3$ is rarely used as an anti-wear or friction reduction additive, it is beneficial as a dopant to play a synergistic role with $MoS_2$ in the solid lubricant coating (Zabinski et al., 1993, 1995; Hu et al., 2006). It was previously reported that the $MoS_2$-$Sb_2O_3$-C film can change its surface with the environment changes to maintain good tribological performance by adapting to the testing conditions (Shirani et al., 2020). In another study it was found the COF of the sputter-deposited amorphous $MoS_2$-$Sb_2O_3$-Au films decreases during sliding in a dry nitrogen environment as a result of $MoS_2$ changing from amorphous to crystalline phase during this process (Scharf et al., 2010). Here, we also observe the synergistic effect of $Sb_2O_3$ and MSH/C as a result of tribochemically-activated material transformation into an amorphous carbon film which could support the easy sliding performance of the system. Our results propose a new solution to high temperature tribological issues.

# EXPERIMENTAL PROCEDURE

## Materials and Film Preparation

Two types of the powders, MSH/C and antimony oxide ($Sb_2O_3$) were used to produce the coatings. The preparation details on the MSH/C powders could be found in our previous works (Gao et al., 2018a). Shortly, the powders were prepared by magnetic stirring a mixture of MgO and $SiO_2$ as raw materials and oleic acid as a carbon source in a subcritical alkaline water environment at 300°C for 48 h. Antimony trioxide ($Sb_2O_3$) powders of ∼5 μm in diameter were purchased from HiMedia (AR, CAS No. 1309-64-4).

The coatings used in this study were produced by burnishing powders onto a substrate surface. The burnishing process is a room-temperature mechanical, which uses balls or rollers to press lubricant powders on the surface (Hassan and Al-Bsharat, 1996). As for the film preparation, the specimen (Inconel IN718 substrate of 25 mm in diameter) was fixed on the rotating platform, and 0.011 g $Sb_2O_3$ was added during the rotation process. The substrate disk was polished before the burnishing process to the roughness Sa of 0.009 μm (**Supplementary Figure 1**). The rotation speed and force were adjusted during the burnishing process. Instead of using ball or pins, we used a lint free cloth to burnish. In the initial stage, the force and rotation speed were changed in the range of 1–5 N and 10–50 RPM, respectively. After obtaining the film, the force and rotation speed increased to 5–10 N, 100–200 RPM. As a result, $Sb_2O_3$ has been evenly distributed on the specimen surface thus forming a uniform adhesion layer. After obtaining the dense $Sb_2O_3$ layer on the surface, a layer of MSH/C (0.003 g) was uniformly spread on the surface by the same method.

**TABLE 1** | The experimental details.

| Label | Load-Speed | Temperature | Revolutions | Materials |
|---|---|---|---|---|
| $Sb_2O_3$ | 0.59 N-10 rpm | RT | 500 cycles | $Si_3N_4$-IN718 |
| $Sb_2O_3$ | 0.59 N-10 rpm | 200°C | 500 cycles | $Si_3N_4$-IN718 |
| $Sb_2O_3$ | 0.59 N-10 rpm | 300°C | 500 cycles | $Si_3N_4$-IN718 |
| $Sb_2O_3$-MSH/C | 0.59 N-10 rpm | RT | 500 cycles | $Si_3N_4$-IN718 |
| $Sb_2O_3$-MSH/C | 0.59 N-10 rpm | 200°C | 500 cycles | $Si_3N_4$-IN718 |
| $Sb_2O_3$-MSH/C | 0.59 N-10 rpm | 300°C | 500 cycles | $Si_3N_4$-IN718 |
| $Sb_2O_3$-MSH/C | 0.59 N-10 rpm | Variable Temp | 500 cycles | $Si_3N_4$-IN718 |

## Friction Test

The friction tests were carried out using Nanovea T50 high temperature pin-on-disk tribometer. During the tests, the temperature of the samples and counterparts varied from 25°C (RT) up to 300°C using the high-temperature furnace operating under open air conditions. The friction pair was composed of a $Si_3N_4$ ball (diameter: 6 mm) and a sample of an MSH/C-based coating on the inconel (IN718) substrate (diameter: 25 mm). Before the test, the $Si_3N_4$ balls were cleaned by acetone followed by isopropyl alcohol. For the high-temperature test, the samples were heated at 2°C/min heating rate up to the target temperature and kept at the target temperature for at least 15 min prior to starting the tribo tests. Based on the preliminary tribological assessment of the burnished samples the testing parameters were adjusted as following: applied load was 0.59 N (corresponding to the maximum Hertz contact stress of 0.35 GPa), the rotational speed was 10 rpm, and the wear track radius was 4 mm. The used parameters are summarized in **Table 1**.

## Characterization

After the test, the width of the wear scars and wear marks were directly observed and measured using a Zeiss optical microscope. The surface imaging of the samples before the measurements and after the tribotests was performed using Hitachi TM3030 scanning electron microscope (SEM) with energy dispersive x-ray spectroscopy (EDS) analysis. Raman characterization of the

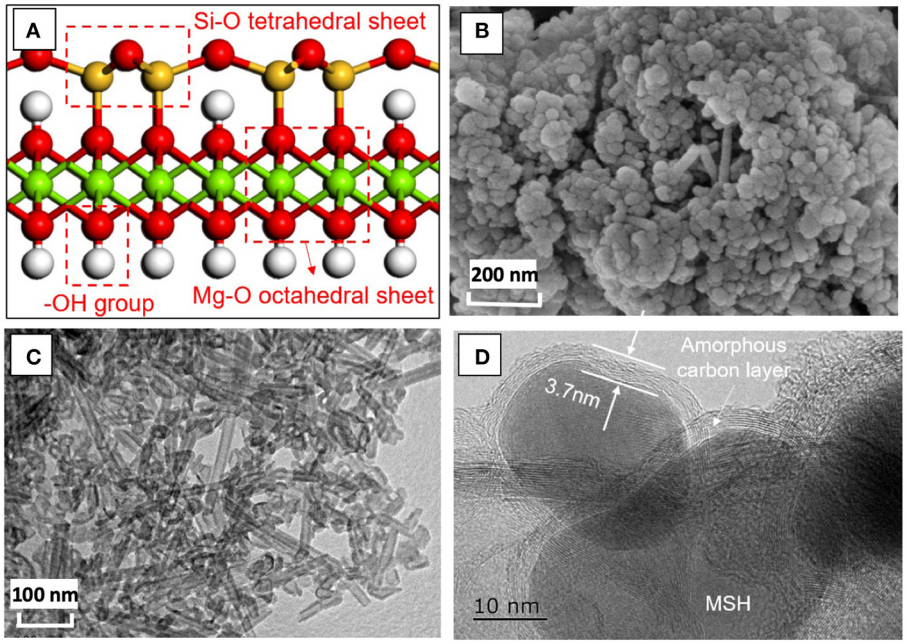


**FIGURE 1 |** The **(A)** crystal structure, **(B)** SEM, **(C)** TEM images of MSH/C composite powders used in the solid film. **(D)** High resolution TEM analysis of the powders indicates presence of amorphous carbon layer on the MSH/C particle surface.

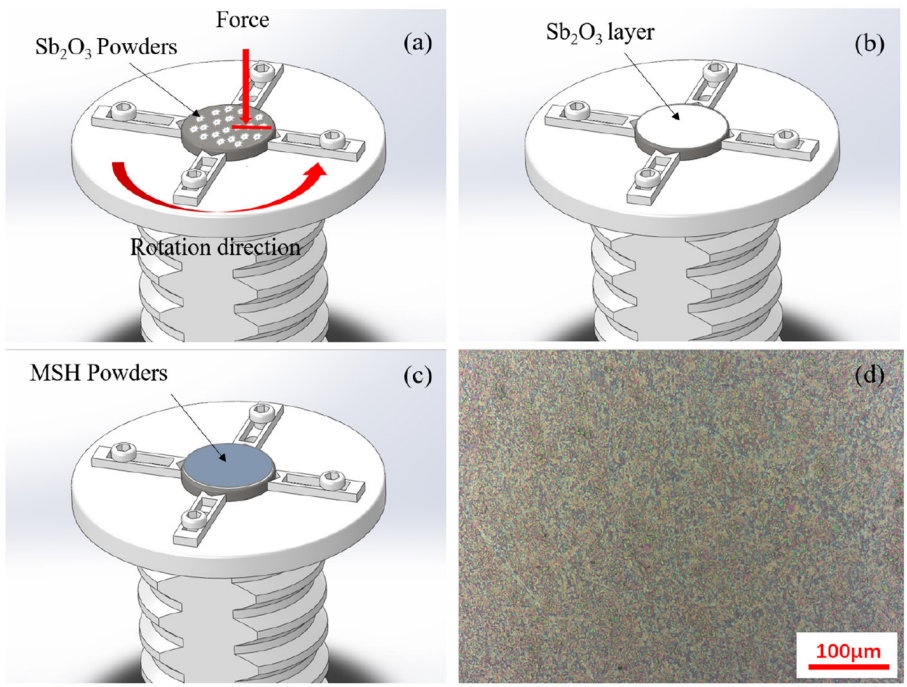


**FIGURE 2 |** The diagram of the film preparation process: **(a)** antimony oxide powder is first used to create **(b)** a uniform adhesion layer that is then covered with **(c)** the MSH/C powder-based film. **(d)** SEM image indicates uniform coverage of the final sample surface.

films was performed with Renishaw confocal Raman system (green laser) equipment with a home-built high temperature extension probe connected to the fiber optics attachment (the sampling beam size was 2 mm in diameter). Transmission electron microscopy (TEM) analysis was performed using FEI Technai G2 F20. X-ray photoelectron spectroscopy (XPS)

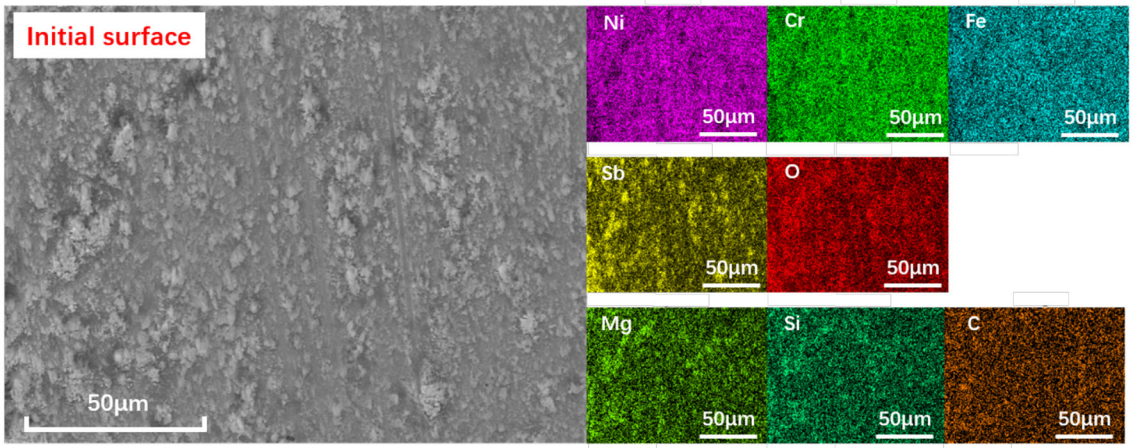


**FIGURE 3 |** The SEM and the elemental mapping images of as-prepared $Sb_2O_3$-MSH/C surface. High uniformity of the particle distribution on the surface is observed.

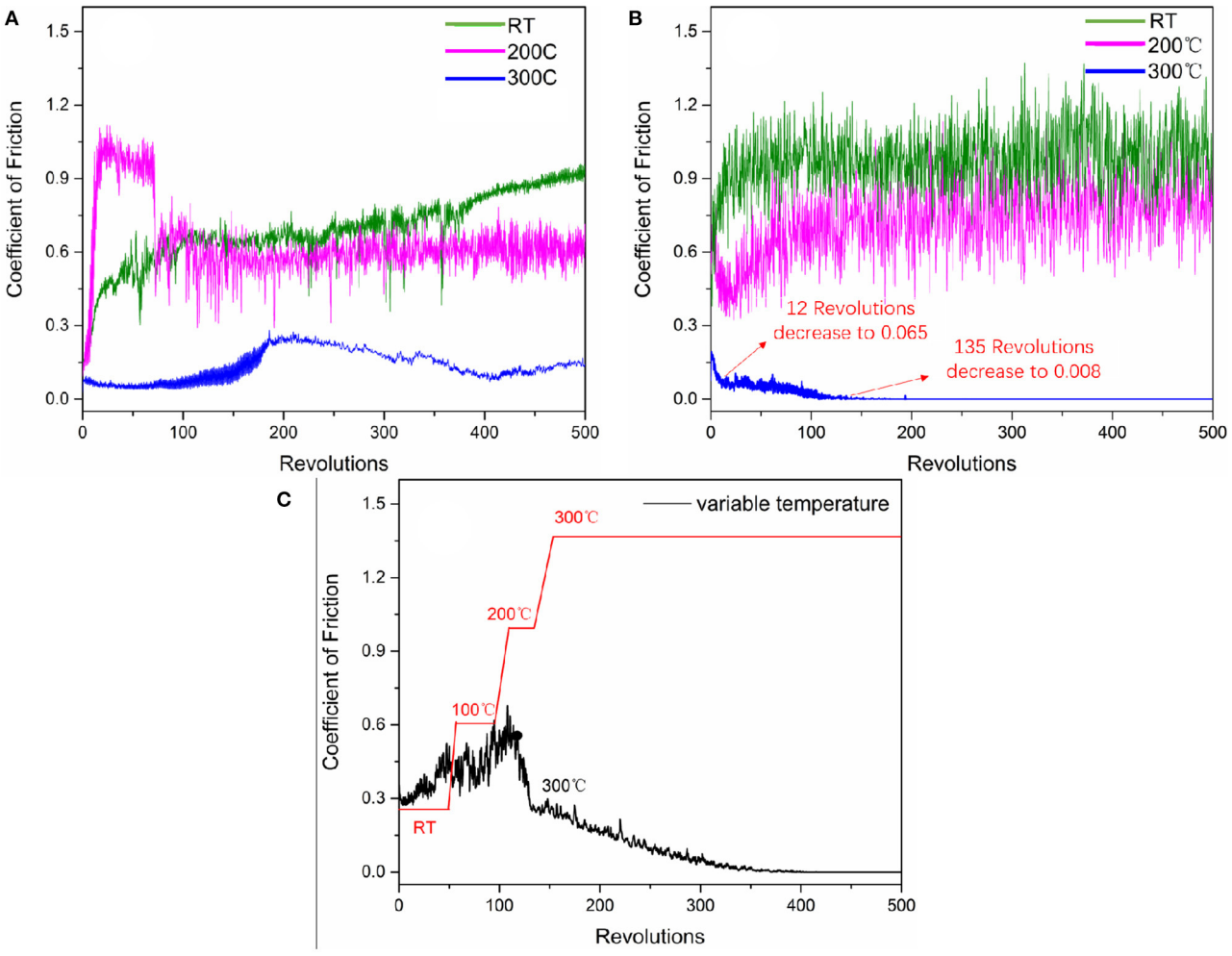


**FIGURE 4 |** COF behavior of **(A)** $Sb_2O_3$, **(B)** $Sb_2O_3$-MSH/C coatings tested under different temperature comdition, and **(C)** $Sb_2O_3$-MSH/C coating continuously monitored during temperature ramping from the RT up to 300°C. Due to the limitation of furnace power, the heating rate for the temperature ranges of RT-100°C, 100–200°C, 200–300°C has been changed from 2.08°C/s to 1.11°C/s, and 0.83°C/s, respectively.

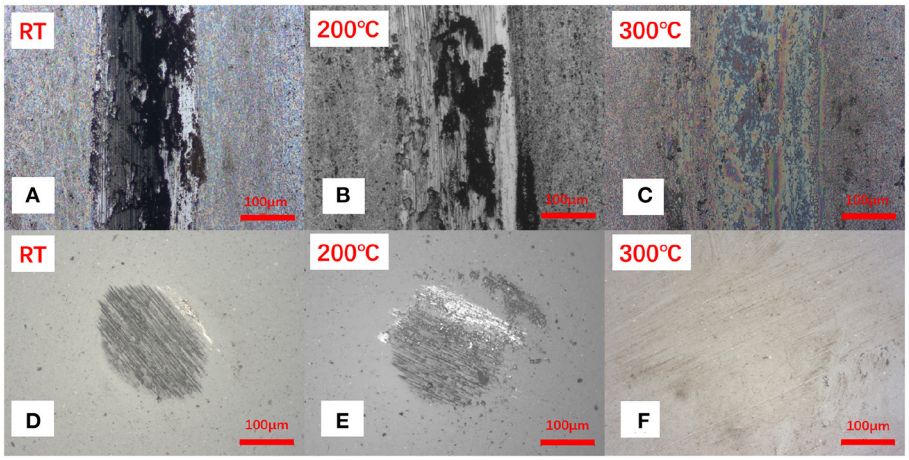


**FIGURE 5 |** The optical images of **(A–C)** worn tracks, **(D–F)** corresponding ball worn surfaces for the $Sb_2O_3$-MSH/C sample after the tribotests performed under different temperature conditions.

analysis was performed using a PHI 5000 Versaprobe Scanning X-ray Spectrometer.

## RESULTS AND DISCUSSION

The coatings used in this study were designed using MSH/C powders (**Figure 1**). The final crystal structure (**Figure 1A**) of the powders indicates that they are composed of Si-O tetrahedral layer, Mg-O octahedral layer, and -OH group (Dixon, 1989; Zhao et al., 2012). Scanning electron microscopy (SEM) and TEM images indicate the the MSH/C poswders are the mixtures of granular and tubular shape particulates with diameter of ∼30–50 nm and the tube length reaching hundreds of nanometers (**Figures 1B,C**). Transmission electron microscopy images also confirm that the particles are coated with an amorphous carbon layer with a thickness of several nanometers as indicated in **Figure 1D**.

The powders were used for coating the inconel substrates using the burnishing process. The schematic of the process and the final surface morphology are shown in **Figures 2a–d**. The average surface roughness of the coatings after burnishing was about 0.27 μm (**Supplementary Figure 2**). And the thickness of the prepared film was ∼1 μm (**Supplementary Figure 3**). The hardness values for the inconel substrates and $Sb_2O_3$ and $Sb_2O_3$-MSH/C coatings were about 6.39, 2.517, and 2.196 GPa, respectively (tested by a nanoindentation tester, **Supplementary Figure 4**).

The morphology and element distribution of as-prepared surfaces are shown in **Figure 3**. It can be seen that all the elements on the surface can be divided into three groups: Ni, Cr, and Fe belonging to the substrate material; Sb and O elements belonging to the $Sb_2O_3$ layer; and Mg, Si, O, and C belonging to the MSH/C composite nanoparticles. Note that $Sb_2O_3$ film prepared by the burnishing process is not uniformly distributed. Except for the layer on the surface, there are a large number of small $Sb_2O_3$ peaks in the form of aggregates, making the surface uneven. The presence of MSH/C composite nanoparticles is higher in the depression area composed of rough peaks, which is confirmed by the distribution of Mg and Si elements: except for the layer of MSH/C present on the surface, a significant increase in the content of Mg and Si elements was observed in the area surrounding the $Sb_2O_3$ peaks.

Designed coatings, after burnishing with $Sb_2O_3$ (labeled as $Sb_2O_3$) and after burnishing with $Sb_2O_3$ and MSH/C (labeled as $Sb_2O_3$-MSH/C) powders, were tested for their tribological performance. The COF results for the coatings tested at different temperatures are shown in **Figures 4A,B**. For the $Sb_2O_3$ coating, room temperature and 200°C tests resulted in considerably high COF values, 0.9 and 0.6 correspondingly. Meanwhile, further increase in the temperature to 300°C led to the COF reduction to 0.15. Such a decrease is attributed to elimination of water vapors adsorbed on the sample from the humid environment during burnishing process. After adding the MSH/C, the COF value was still high at room temperature and 200°C, reaching 0.95 and 0.8, respectively. However, as the temperature further increased to 300°C, the COF demonstrated rapid decrease after starting the test. After ∼12 revolutions, the COF had dropped to 0.065. Further testing resulted in the COF showing a slow downward trend, and after 135 revolutions, the friction coefficient dropped to 0.008, thus entering the superlubricity region.

To further test the temperature sensitivity of the friction behavior of the coating, we continuously monitored the friction behavior while increasing the temperature from RT up to 300°C. The results indicated similar trend in the COF decrease under the elevated temperature conditions with friction approaching superlubricity values once the system reaches the higher temperature regime (**Figure 4C**). In the first 50 revolutions performed at RT, the COF continued to increase; ramping the temperature up to 100°C during additional 50 revolutions resulted in a more sporadic COF behavior around 0.4–0.5. Once the temperature reached 200°C, the COF dropped rapidly,

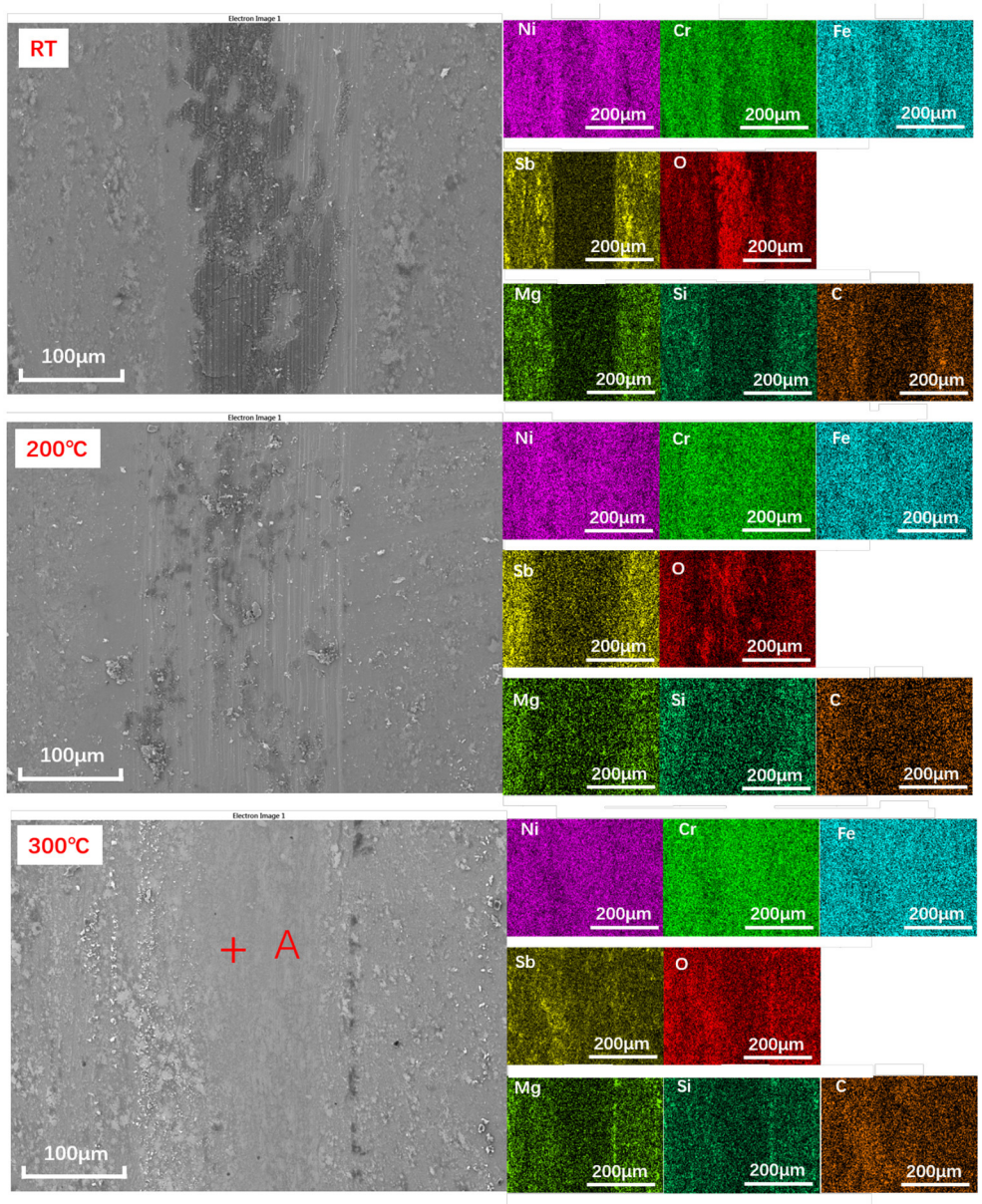


**FIGURE 6 |** The SEM and EDS elemental mapping images of the $Sb_2O_3$-MSH/C wear track areas formed during the tribotests performed under different temperature conditions. Point A was selected for the XPS analysis.

changing from 0.63 to 0.25 within 38 revolutions. As the temperature increased further to 300°C over 150 revolutions, the COF continued to decrease steadily, and finally decreased to 0.008 at 400 revolutions, entering the superlubricity region.

To understand the origin of such behavior, we analyzed the wear tracks produced on the samples. Optical images of the wear scars and wear marks clearly show a difference when transitioning from the RT to the elevated temperature (**Figure 5** and **Supplementary Figure 5**). While the high temperature tests indicate very mild wear of the materials, exposure of the samples to the lower temperature tests results in significant wear of the coatings. The micrographs suggest that under room temperature conditions the coating has been removed completely from the wear track during sliding resulting in the formation of a blackish film materials. The samples were further subjected to the SEM analysis suggesting that the blackish film is higher in the oxygen concentration, perhaps related to the metal oxide formed during sliding, rather than the coating materials (**Figure 6** and **Supplementary Figure 6**).

As a result of lacking protective layer, large amounts of scratches appeared on the corresponding ball surface. As the temperature increased to 200°C, although more Sb, Mg, Si

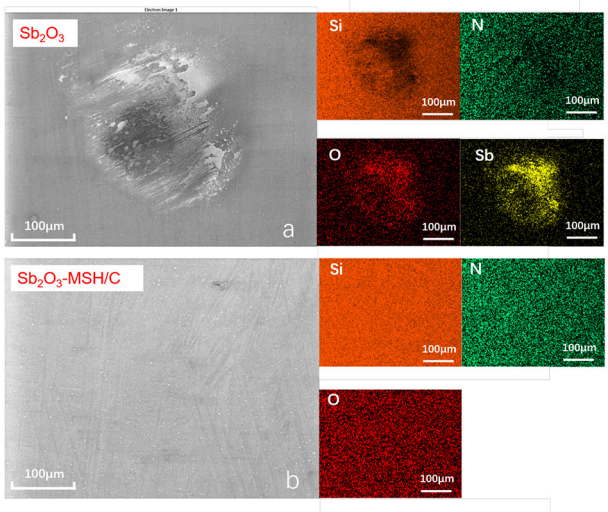


**FIGURE 7 |** The SEM and the corresponding EDS elementap mapping images of the wearmarks for the silicon nitride balls after the tests performed at 300°C for **(a)** $Sb_2O_3$ and **(b)** $Sb_2O_3$-MSH/C samples.

elements could be detected on the $Sb_2O_3$-MSH/C wear track area, the major part of the film has been worn out from the contact area, exposing the substrate surface and generating large amounts of oxidation products and scratches. However, when the tests were performed at 300°C, the wear track area was still covered by a $Sb_2O_3$-MSH/C layer even after the whole duration of the test, as shown in **Figure 6**. These results suggest that uniform coverage of the MSH/C film prevented exposure of the substrate to the sliding, thus inhibiting formation of the scratches and oxidation of the substrate materials. Evenmore, with the temperature increase, presence of the oxide products on the surface of the wear mark substantially decreased. This suggests that there is a synergy of protective properties of the $Sb_2O_3$ and MSH/C layers that do not only isolate the direct contact of friction pairs but also protect the substrate material from the oxidation. Analysis of the $Si_3N_4$ ball surfaces after the $Sb_2O_3$ tests indicated no obvious signs of wear but rather transfer of the protective coating to promote beneficial tribological characteristics of the films (**Figure 7**). Note that in case of $Sb_2O_3$-MSH/C, no obvious material transfer, such as $Sb_2O_3$ or carbon layer, is observed (**Figure 7b** and **Supplementary Figure 7**). This suggests that the composite film shows overall better integrity and the generated transfer film is weakly bonded to the silicon nitride surface and is easily wiped of during the post-processing. Therefore, the low-friction sliding at 300°C mostly occurs at the interfaces formed between MSH-generated carbon film and the silicon nitride ball surface. Similar wear-free behavior of the silicon nitride ball in contact with the diamond-like carbon (DLC) surface has been observed before by Jia et al. (1995).

Our results indicate that temperature plays an important role in the realization of superlubricity. Antimony trioxide ($Sb_2O_3$) itself still shows relatively high COF values suggesting that the $Sb_2O_3$ surface prepared by the burnishing process is rough with large number of $Sb_2O_3$ peaks being formed. Consequently, prolonged duration of the tests may lead to the complete removal of the top $Sb_2O_3$ layer and exposure of the metal substrate, which could cause high COF values and severe wear of the tribopairs. Observed decrease in the COF value at 300°C proved high temperature could be beneficial to the friction reduction.

We further probed the origin of temperature effect by *in-situ* Raman analysis of the coatings while heating (**Figure 8**). For Raman characterization of $Sb_2O_3$ film (**Figure 8a**), the measurement parameters and measurement positions were kept the same for the tested different temperatures. Resulting spectra indicate presence of six Raman peaks in the range of 150–950 $cm^{-1}$: the peaks at 190 and 451 $cm^{-1}$ come from the bending mode of Sb-O-Sb while the peaks at 255, 356, 373, and 714 $cm^{-1}$ correspond to the stretching mode of Sb-O-Sb (Zeng et al., 2004). It can be seen that with the temperature increase, the intensity of each Raman peak gradually decreases, suggesting decrease in the corresponding vibrational groups. These results are in agreement with previously reported studies (Naidu et al., 2009) reporting that with the increase of temperature from room temperature and up to 400°C, the intensities of diffraction peak corresponding to $Sb_2O_3$ (110) crystal plane and (200) crystal plane gradually decrease, indicating that the crystal is gradually destroyed. The results suggest that such structural changes affect the adhesion of $Sb_2O_3$ to the metal substrate, thus reducing the direct contact of the tribopairs. Because of the $Sb_2O_3$ being used to improve the adhesion of the MSH/C layer to the substrate material, more MSH/C could be involved the friction reduction process. Thus, $Sb_2O_3$ provides support for the lubricant to remain at the sliding interface. Considering the combined storage and support role of $Sb_2O_3$ demonstrated by the presence of the rough peaks on the MSH/C powder shown in **Figures 8c,d**, the worn surface could still be covered by a layer of lubricant. Meanwhile, the addition of top MSH/C also protects the bottom $Sb_2O_3$ layer, which, as reflected by the mapping results at 200°C, results in more Sb being detected on the $Sb_2O_3$-MSH/C than on the $Sb_2O_3$ surface thus supporting the findings in **Figure 6** and **Supplementary Figure 6**.

We evaluated the necessity of the MSH/C presence for achieving superlubricity under high temperature conditions. The Raman results of MSH/C under different temperatures reflected the changes in the MSH/C crystal structure upon temperature increase, as shown in **Figure 8b**. The -O-H vibration peak located at 229 $cm^{-1}$ and the Si-O-Si peak located at 691 $cm^{-1}$ disappeared after temperature reaching 300°C. Besides, the intensity of the $SiO_4$ symmetrical stretching vibration peak at 386 $cm^{-1}$ also decreased significantly. This indicates that the -O-H and Si-O bonds in the MSH/C powders are destroyed with the temperature increase, thus leading to the release of a large amount of Si-O and -OH groups. The TG-DSC results in our pervious work also confirmed the release of -OH group (also called as the stuctural water) with the increase of temperature (Gao et al., 2018b). These active groups released from the MSH/C powders are the key reason for their excellent tribological performance (Chang et al., 2017, 2019). Local heating induced by friction is expected to further

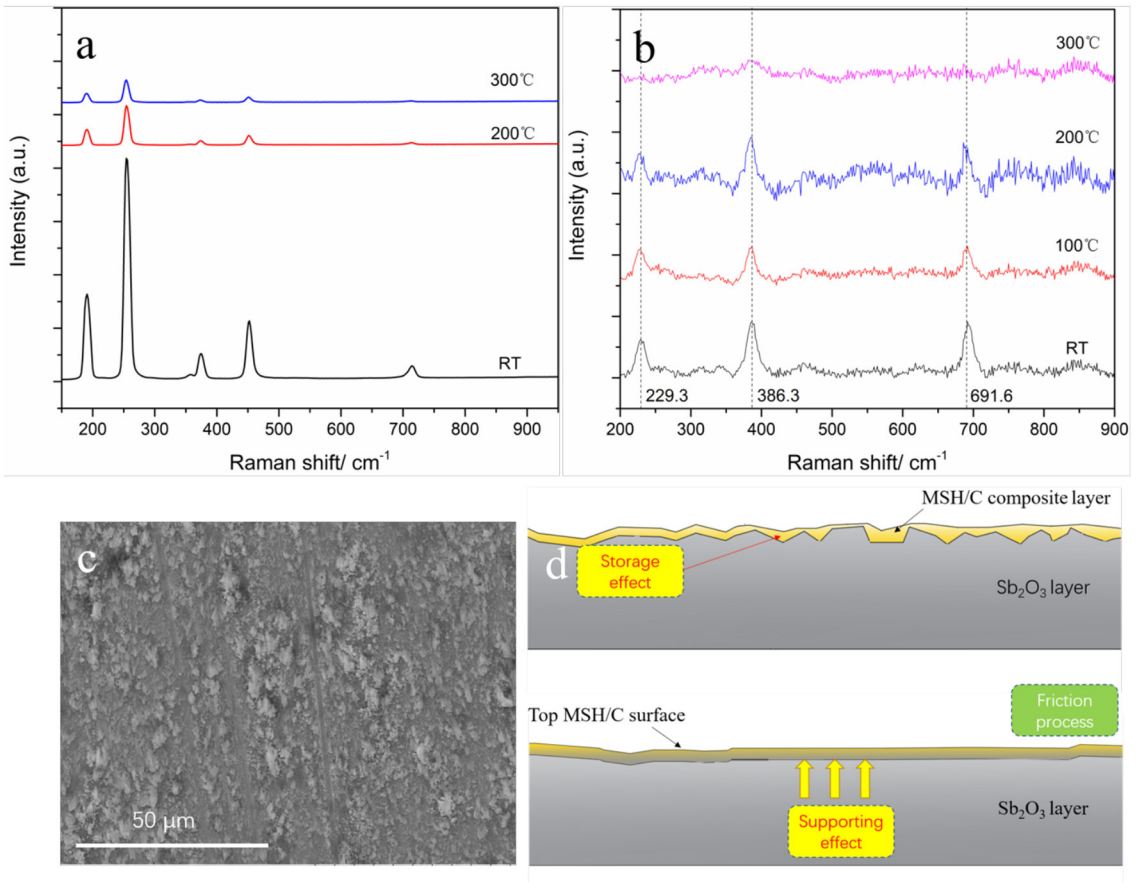


**FIGURE 8 |** Raman spectrums of $Sb_2O_3$ **(a)** and MSH/C **(b)** under different temperatures (Excitation wavelength of 532nm) used for the tribological analysis, **(c)** the rough surface prepared by burnish process, and **(d)** the synergistic effect between the MSH/C layer and $Sb_2O_3$ layer.

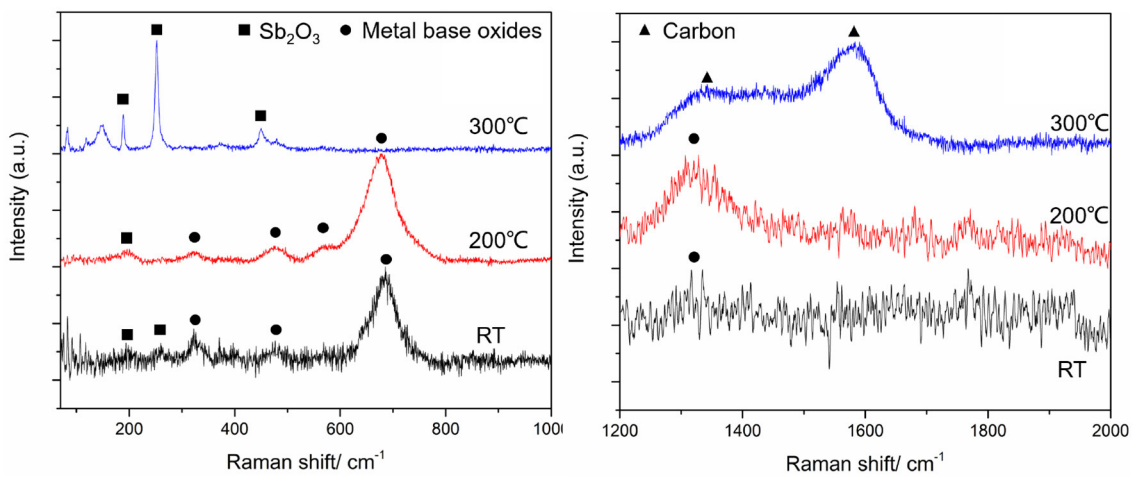


**FIGURE 9 |** Raman results of the worn $Sb_2O_3$-MSH/C surfaces under different temperature conditions.

promote the decomposition of the MSH/C and the release of various active groups. Considering the mild tribological test condition (0.59 N−10 rpm) used in our study, the MSH/C could present the best performance under 300°C since the heat conduction energy will make up for the lack of friction energy.

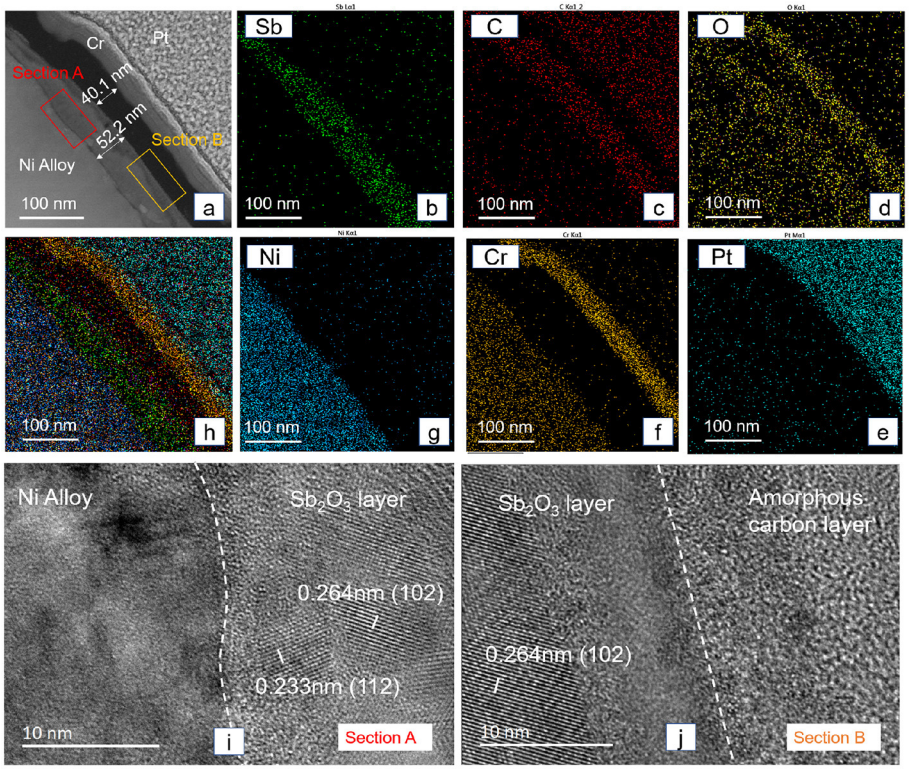


**FIGURE 10 |** Cross-sectional TEM image of the $Sb_2O_3$-MSH/C surface after the test under 300°C **(a)**, the EDS elemental mapping of the cross-sectional area **(b–h)**, and High-resolution TEM image is taken from the interface area of different layers **(i, j)**, which is also marked as section A and section B in **(a)**. The Pt and Cr protective layers were deposited to protect the tribofilm from the damage during TEM specimen preparation.

In addition to the analysis of the properties of the powders at different temperatures, we have carried out a more in-depth analysis of the coating surfaces after the tests. The Raman results of worn surfaces under different temperatures are shown in **Figure 9**. It can be noticed that under RT and 200°C, due to the large removal of the $Sb_2O_3$-MSH/C layer in the friction process, the metal substrate is exposed to sliding causing formation of oxides as it is confirmed by the presence of various metal oxide Raman peaks, including iron oxide (323 $cm^{-1}$) (de Faria et al., 1997), nickel oxides (476, 560 $cm^{-1}$) (Nan et al., 2006; Kumar et al., 2020), and chromium oxides (680 $cm^{-1}$) (Guinneton et al., 2005). Besides, the $Sb_2O_3$ peak located at 190 $cm^{-1}$, a new peak at 255 $cm^{-1}$ also appeared, though its intensity is weak. No carbon or MSH related Raman peaks could be found on the worn surfaces. However, in case of 300°C test, strong Sb-O vibration peaks located at 190 and 255 $cm^{-1}$ appeared, which further proved better integrity of the coating at higher temperature and better survivability of $Sb_2O_3$ on the metal surface. Meanwhile, during sliding at the lower temperatures, $Sb_2O_3$ does not have strong enough adhesion to the substrate and the coating does not remain intact during sliding. Importantly, high temperature test at 300°C also indicated presence of the carbon G peak and D peak located at 1,583 and 1,340 $cm^{-1}$ respectively, that were not observed for the coatings heated but without being subjected to the shear stresses. It is worth to mention that the D peak shifts toward the low wavenumber with the influence of the Si element (Veres et al., 2006).

The structure and composition of the tribofilm formed on the $Sb_2O_3$-MSH/C coating at 300°C were analyzed using the TEM analysis. For this, we use the Focused Ion Beam (FIB) technology to prepare a samples from the worn surface of $Sb_2O_3$-MSH/C after the test (**Figure 10**). The cross-sectional TEM image in **Figure 10a** and mapping results in **Figures 10b–h** indicate the existence of a $Sb_2O_3$ layer and an amorphous carbon layer with thicknesses reaching 52.2 and 40.1 nm, respectively. In contrast to the layered structure of the carbon layer observed in **Figure 1D**, the formed tribofilm is mostly of the amorphous nature. The High-resolution TEM image of Section A in **Figure 10i** shows the borderline between alloy base and $Sb_2O_3$ layer. Nanocrystalline structure and amorphous structure both existed in this $Sb_2O_3$ layer. Interestingly, the border section is occupied by the amorphous $Sb_2O_3$, not only in Section A but also in Section B shown in **Figure 10j**, which is the transition region between the $Sb_2O_3$ layer and amorphous carbon layer.

The TEM results of the wear track were complemented by the XPS characterization of the tribofilm surface (**Figure 11**). There was no obvious signal of Fe, Ni and other elements belonging to the metal substrate in **Figure 11**, which indicates the metal matrix is not exposed during the friction process. The worn surface is mainly composed of C, O, and Sb elements with the

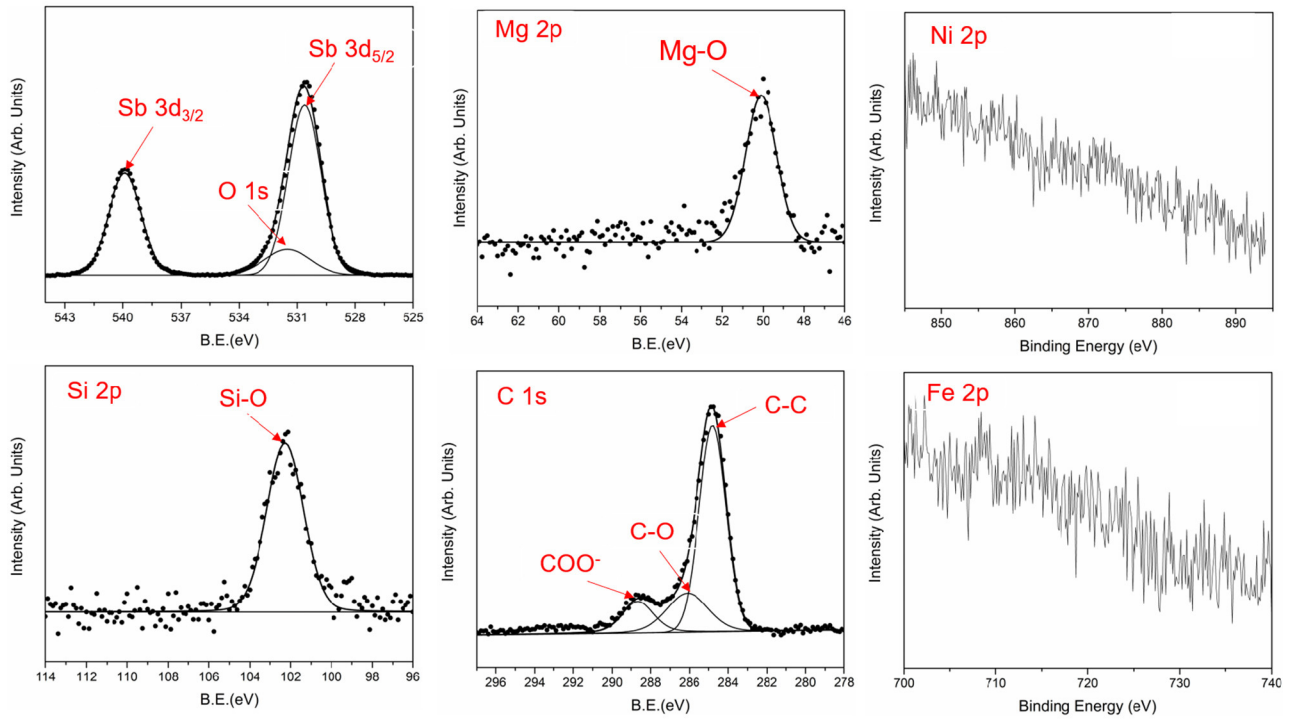


**FIGURE 11 |** XPS spectra of the elements on the wear track area of $Sb_2O_3$-MSH/C under 300°C (point A in **Figure 6**).

elemental concentration (at.%) of 24.7, 62.2, and 7.6%, which is in agreement with the TEM results: an outer carbon layer, an inner $Sb_2O_3$ layer. The amorphous carbon layer in **Figure 10j** is made up of C-C, C-O, and $COO^-$ as the C 1s peak can be fitted by three peaks at 284.8, 286.1, and 288.6 eV (Grzybek et al., 2004; Morent et al., 2008; Cai and Zhang, 2013; Samanta et al., 2019). The C-C bond only accounted for 66.1%, which indicates the oxidation reaction takes place in the process of high temperature friction resulting in about third of C atoms being bonded with O atoms to form C-O and O-C=O groups. The O 1s peak at 531.5 eV is covered by Sb $3d_{5/2}$ at 530.6 eV, but it can be separated by the rules, such as the equal half peak width, the peak distance (9.3 eV), and the relative area ratio (1.5) between Sb $3d_{5/2}$ peak and Sb$3d_{3/2}$ peak that is centered at 539.9 eV (Honma et al., 2000; Huang and Ruiz, 2005). In addition, Mg and Si are also detected on the surface of the tribofilm, though at much lower concentration: Mg 2p 2.1%, Si 2p 3.2%, existing in the form of Si-O-C and Mg-O (Ardizzone et al., 1997; Jantschner et al., 2015; Zhang et al., 2020), which indicates the decomposition of in the friction process.

Overall, the characterization results suggest that during sliding the carbon initially covering the MSH surface has been tribochemically converted to a more disordered amorphous carbon layer protecting the underlying substrate. At the same time, the structural transformation has been accompanied by the oxidation induced by the open air conditions and MSH chemistry and accelerated by high temperature. Previously it has been shown that during sliding the MSH crystals tend to decompose, releasing Si-O, Mg-O, and -OH active groups which could promote formation of the oxide layer as the lubricating oil addtive (Wang et al., 2020). Here, in dry sliding conditions, these MSH-based active groups could cause the formation of the Si-O-C bonds (Jantschner et al., 2015). The tribochemically-activated formation of the composite amorphous carbon layer doped with Si and O on the surface of $Sb_2O_3$ is the key to reducing of the COF and achieving the superlubricity at 300°C, which has been confirmed earlier (Jantschner et al., 2014, 2015; Evaristo et al., 2016). The thermomechanical process also promotes healing of the creacks and defects in the film and improves the coating resistance to fracture and fatigue in the high-temperature contact. M. Evaristo et al. found that the incorporation of Si and O in the amorphous carbon layer can reduce the friction coefficient from 0.17 to 0.034 (Evaristo et al., 2016). O. Jantschner et al. pointed out that the addition of a small amount of Si (< 5 at.%) to the amorphous carbon coating at 240–450°C also beneficially affects the tribological performance of the film [the COF was reduced from 0.3 (amorphous carbon) to < 0.02] (Jantschner et al., 2014, 2015). Although the mechanism of friction reduction with Si and O doping is not clear, it is assumed the formation of Si-O-C compounds in the sliding surface could help protect the surface near C=O, thus inducing easier sliding at the interfaces (Jantschner et al., 2015).

## CONCLUSION

In conclusion, we designed a new MSH/C-based coating using burnishing process. While the friction remained relatively high

during the room temperature tests, our analysis indicated excellent tribological performance of the coating when tested at elevated temperature of 300°C. The wear track analysis suggests that the origin of such high temperature behavior of the coating can be attributed to the formation of low-friction tribofilm that is enabled by tribochemically-induced formation of carbon layer on the surface of the coating. This film provides better protection of the surface during sliding and prevents material wear or transfer to the counterpart surface.

High temperature *in-situ* Raman analysis of the films further supported the findings of the study suggesting that the superlibric nature of the coating is a synergistic effect of the antimony oxide adhesion layer, tribochemically-active MSH powders, and tribochemically-generated surface carbon film.

Our results provide new insights into high temperature lubrication systems that can be easily self-repaired by supplying the materials to the sliding contacts through the burnishing process.

## DATA AVAILABILITY STATEMENT

The raw data supporting the conclusions of this article will be made available by the authors, without undue reservation.

## AUTHOR CONTRIBUTIONS

KG: investigation, data curation, and writing. BW and AS: data curation. QC: resources. DB: supervision, investigation, conceptualization, and writing. All authors contributed to the article and approved the submitted version.

## FUNDING

This work was funded by National Science Foundation (Award No. 2018132).

## ACKNOWLEDGMENTS

The authors acknowledge support of this work by the National Science Foundation (NSF) (Award No. 2018132). This work was performed in part at the University of North Texas' Materials Research Facility.

## SUPPLEMENTARY MATERIAL

The Supplementary Material for this article can be found online at: https://www.frontiersin.org/articles/10.3389/fchem.2021.667878/full#supplementary-material

## REFERENCES

Aouadi, S. M., Gu, J., and Berman, D. (2020). Self-healing ceramic coatings that operate in extreme environments: a review. *J. Vac. Sci. Technol. A* 38:050802. doi: 10.1116/6.0000350

Ardizzone, S., Bianchi, C. L., Fadoni, M., and Vercelli, B. (1997). Magnesium salts and oxide: an XPS overview. *Appl. Surf. Sci.* 119, 253–259. doi: 10.1016/S0169-4332(97)00180-3

Berman, D., Deshmukh, S. A., Sankaranarayanan, S. K. R. S, Erdemir, A., and Sumant, A. V. (2015). Macroscale superlubricity enabled by graphene nanoscroll formation. *Science* 348, 1118–1122. doi: 10.1126/science.1262024

Berman, D., Erdemir, A., and Sumant, AV. (2018a). Approaches for achieving superlubricity in two-dimensional materials. *ACS Nano.* 12, 2122–2137. doi: 10.1021/acsnano.7b09046

Berman, D., Mutyala, K. C., Srinivasan, S., Sankaranarayanan, S. K. R. S., Erdemir, A., Shevchenko, E. V., et al. (2019). Iron-nanoparticle driven tribochemistry leading to superlubric sliding interfaces. *Adv. Mater. Interfaces* 6:1901416. doi: 10.1002/admi.201901416

Berman, D., Narayanan, B., Cherukara, M. J., Sankaranarayanan, S. K. R. S., Erdemir, A., Zinovev, A., et al. (2018b). Operando tribochemical formation of onion-like-carbon leads to macroscale superlubricity. *Nat. Commun.* 9:1164. doi: 10.1038/s41467-018-03549-6

Cai, C. C., and Zhang, M. X. (2013). XPS analysis of carbon and oxygen in coking coal with different density intervals. *Appl. Mech. Mater.* 347–350, 1239–1243. doi: 10.4028/www.scientific.net/AMM.347-350.1239

Chang, Q., Rudenko, P., Miller, D. J., Wen, J., Berman, D., Zhang, Y., et al. (2017). Operando formation of an ultra-low friction boundary film from synthetic magnesium silicon hydroxide additive. *Tribol. Int.* 110, 35–40. doi: 10.1016/j.triboint.2017.02.003

Chang, Q. Y., Wang, B., and Gao, K. (2019). Pressure-dependent anti-wear mechanisms of synthetic magnesium silicate hydroxide nanoparticles. *Tribol. Int.* 135, 230–236. doi: 10.1016/J.TRIBOINT.2019.03.016

de Faria, D. L. A., Venâncio Silva, S., and de Oliveira, M. T. (1997). Raman microspectroscopy of some iron oxides and oxyhydroxides. *J Raman Spectrosc* 28, 873–878. doi: 10.1002/(SICI)1097-4555(199711)28:11<873::AID-JRS177>3.0.CO;2-B

Dienwiebel, M., Verhoeven, G. S., Pradeep, N., Frenken, J. W. M., Heimberg, J. A., and Zandbergen, H. W. (2004). Superlubricity of graphite. *Phys. Rev. Lett.* 92:126101. doi: 10.1103/PhysRevLett.92.126101

Dixon, J. B. (1989). Kaolin and serpentine group minerals. *Miner. Soil Environ.* 1, 467–519. doi: 10.2136/sssabookser1.2ed.c10

Evaristo, M., Azevedo, R., Palacio, C., and Cavaleiro, A. (2016). Influence of the silicon and oxygen content on the properties of non-hydrogenated amorphous carbon coatings. *Diam. Relat. Mater.* 70, 201–210. doi: 10.1016/j.diamond.2016.10.024

Gao, H., Otero-de-la-Roza, A., Gu, J., Stone, D., Aouadi, S. M., Johnson, E. R., et al. (2015). (Ag,Cu)-Ta-O ternaries as high-temperature solid-lubricant coatings. *ACS Appl. Mater. Interfaces* 7, 15422–15429. doi: 10.1021/acsami.5b03543

Gao, K., Chang, Q., Wang, B., Zhou, N., and Qing, T. (2018a). Synthetic magnesium silicate hydroxide nanoparticles coated with carbonaceous shell in subcritical water condition. *Appl. Surf. Sci.* 450, 312–317. doi: 10.1016/j.apsusc.2018.04.139

Gao, K., Chang, Q., Wang, B., Zhou, N., and Qing, T. (2018b). The purification and tribological property of the synthetic magnesium silicate hydroxide modified by oleic acid. *Lubr. Sci.* 2018, 377–385. doi: 10.1002/ls.1428

Grzybek, T., Pietrzak, R., and Wachowska, H. (2004). The comparison of oxygen and sulfur species formed by coal oxidation with $O_2$/$Na_2CO_3$ or peroxyacetic acid solution. XPS Studies. *Energy Fuels* 18, 804–809. doi: 10.1021/ef030153i

Guinneton, F., Monnereau, O., Argeme, L., Stanoi, D., Socol, G., Mihailescu, I. N., et al. (2005). PLD thin films obtained from $CrO_3$ and $Cr_8O_21$ targets. *Appl. Surf. Sci.* 247, 139–144. doi: 10.1016/j.apsusc.2005.01.073

Hassan, A. M., and Al-Bsharat, A. S. (1996). Influence of burnishing process on surface roughness, hardness, and microstructure of some non-ferrous metals. *Wear* 199, 1–8. doi: 10.1016/0043-1648(95)06847-3

Hirano, M., and Shinjo, K. (1993). Superlubricity and frictional anisotropy. *Wear* 168, 121–125. doi: 10.1016/0043-1648(93)90207-3

Honma, T., Sato, R., Benino, Y., Komatsu, T., and Dimitrov, V. (2000). Electronic polarizability, optical basicity and XPS spectra of $Sb_2O_3$-$B_2O_3$ glasses. *J. Non Cryst. Solids* 272, 1–13. doi: 10.1016/S0022-3093(00)00156-3

Hu, J. J., Bultman, J. E., and Zabinski, J. S. (2006). Microstructure and lubrication mechanism of multilayered $MoS_2$/$Sb_2O_3$ thin films. *Tribol. Lett.* 21, 169–174. doi: 10.1007/s11249-006-9035-6

Huang, Y., and Ruiz, P. (2005). Antimony dispersion and phase evolution in the $Sb_2O_3$-$Fe_2O_3$ system. *Phys. Chem. B* 109, 22420–22425. doi: 10.1021/JP053785+

Jantschner, O., Field, S. K., Holec, D., Fian, A., Music, D., Schneider, J. M., et al. (2015). Origin of temperature-induced low friction of sputtered Si-containing amorphous carbon coatings. *Acta Mater.* 82, 437–446. doi: 10.1016/j.actamat.2014.09.030

Jantschner, O., Field, S. K., Music, D., Terziyska, V. L., Schneider, J. M., Munnik, F., et al. (2014). Sputtered Si-containing low-friction carbon coatings for elevated temperatures. *Tribol. Int.* 77, 15–23. doi: 10.1016/j.triboint.2014.04.006

Jha, A. K., Prasad, K., and Prasad, K. (2009). A green low-cost biosynthesis of Sb2O3 nanoparticles. *Biochem. Eng. J.* 43, 303–306. doi: 10.1016/j.bej.2008.10.016

Jia, K., Li, Y. Q., Fischer, T. E., and Gallois, B. (1995). Tribology of diamond-like carbon sliding against itself, silicon nitride, and steel. *J. Mater. Res.* 10, 1403–1410. doi: 10.1557/JMR.1995.1403

Kawai, S., Benassi, A., Gnecco, E., Söde, H., Pawlak, R., Feng, X., et al. (2016). Superlubricity of graphene nanoribbons on gold surfaces. *Science* 351, 957–961. doi: 10.1126/science.aad3569

Kumar, P. R., Prasad, N., Veillon, F., Prellier, W. (2020). Raman spectroscopic and magnetic properties of europium doped nickel oxide nanoparticles prepared by microwave-assisted hydrothermal method. *J. Alloys Compd.* 2020:157639. doi: 10.1016/j.jallcom.2020.157639

Li, H., Wang, J., Gao, S., Chen, Q., Peng, L., Liu, K., et al. (2017). Superlubricity between $MoS_2$ monolayers. *Adv. Mater.* 29:1701474. doi: 10.1002/adma.201701474

Li, H., Wood, R. J., Rutland, M. W., and Atkin, R. (2014). An ionic liquid lubricant enables superlubricity to be "switched on" *in situ* using an electrical potential. *Chem. Commun.* 50, 4368–4370. doi: 10.1039/c4cc00979g

Liu, Z., Yang, J., Grey, F., Liu, J. Z., Liu, Y., Wang, Y., et al. (2012). Observation of microscale superlubricity in graphite. *Phys. Rev. Lett.* 108:205503. doi: 10.1103/PhysRevLett.108.205503

Martin, J. M., Donnet, C., Le Mogne, T., and Epicier, T. (1993). Superlubricity of molybdenum disulphide. *Phys. Rev. B* 48, 10583–10586. doi: 10.1103/PhysRevB.48.10583

Morent, R., De Geyter, N., Leys, C., Gengembre, L., and Payen, E. (2008). Comparison between XPS- And FTIR-analysis of plasma-treated polypropylene film surfaces. *Surf. Interface Anal.* 40, 597–600. doi: 10.1002/sia.2619

Naidu, B. S., Pandey, M., Sudarsan, V., Vatsa, R. K., and Tewari, R. (2009). Photoluminescence and Raman spectroscopic investigations of morphology assisted effects in $Sb_2O_3$. *Chem. Phys. Lett.* 474, 180–184. doi: 10.1016/j.cplett.2009.04.050

Nan, J., Yang, Y., and Lin, Z. (2006). *In situ* photoelectrochemistry and Raman spectroscopic characterization on the surface oxide film of nickel electrode in 30 wt.% KOH solution. *Electrochim. Acta* 51, 4873–4879. doi: 10.1016/j.electacta.2006.01.031

Samanta, S., Yadav, R., Kumar, A., Kumar Sinha, A., and Srivastava, R. (2019). Surface modified C, O co-doped polymeric g-$C_3N_4$ as an efficient photocatalyst for visible light assisted $CO_2$ reduction and $H_2O_2$ production. *Appl. Catal. B Environ.* 259:118054. doi: 10.1016/j.apcatb.2019.118054

Scharf, T. W., Kotula, P. G., and Prasad, S.V. (2010). Friction and wear mechanisms in $MoS_2$/$Sb_2O_3$/Au nanocomposite coatings. *Acta Mater.* 58, 4100–4109. doi: 10.1016/j.actamat.2010.03.040

Shirani, A., Joy, T., Rogov, A., Lin, M., Yerokhin, A., Mogonye, J. E., et al. (2020). PEO-chameleon as a potential protective coating on cast aluminum alloys for high-temperature applications. *Surf. Coat. Technol.* 397:126016. doi: 10.1016/j.surfcoat.2020.126016

Veres, M., Koós, M., Orsós, N., Tóth, S., Füle, M., Mohai, M., et al. (2006). Incorporation of Si in a-C:Si:H films monitored by infrared excited Raman scattering. *Diam. Relat. Mater.* 15, 932–935. doi: 10.1016/j.diamond.2005.10.051

Wang, B., Chang, Q., Gao, K., Wen, X., Bai, P., Tian, Y. (2020). Superlow wear realizable tribofilms from lubricant oil containing hydrothermally synthesized magnesium silicate hydroxide/carbon core–shell nanoplates. *Langmuir*. 37, 240–248. doi: 10.1021/acs.langmuir.0c02845

Wang, W., Xie, G., and Luo, J. (2018a). Black phosphorus as a new lubricant. *Friction* 6, 116–142. doi: 10.1007/s40544-018-0204-z

Wang, W., Xie, G., and Luo, J. (2018b). Superlubricity of black phosphorus as lubricant additive. *ACS Appl. Mater. Interfaces* 10, 43203–43210. doi: 10.1021/acsami.8b14730

Yu, H., Xu, Y., Shi, P., Wang, H., Wei, M., Zhao, K., et al. (2013). Microstructure, mechanical properties and tribological behavior of tribofilm generated from natural serpentine mineral powders as lubricant additive. *Wear* 297, 802–810. doi: 10.1016/j.wear.2012.10.013

Yu, H. L., Xu, Y., Shi, P. J., Wang, H. M., Zhao, Y., Xu, B. S., et al. (2010). Tribological behaviors of surface-coated serpentine ultrafine powders as lubricant additive. *Tribol. Int.* 43, 667–675. doi: 10.1016/j.triboint.2009.10.006

Zabinski, J. S., Donley, M. S., and McDevitt, N. T. (1993). Mechanistic study of the synergism between $Sb_2O_3$ and $MoS_2$ lubricant systems using Raman spectroscopy. *Wear* 165, 103–108. doi: 10.1016/0043-1648(93)90378-Y

Zabinski, J. S., Donley, M. S., Walck, S. D., Schneider, T. R., and McDevitt, N. T. (1995). The effects of dopants on the chemistry and tribology of sputter-deposited $MoS_2$ films. *Tribol Trans* 38, 894–904. doi: 10.1080/10402009508983486

Zeng, D. W., Xie, C. S., Zhu, B. L., and Song, W. L. (2004). Characteristics of $Sb_2O_3$ nanoparticles synthesized from antimony by vapor condensation method. *Mater. Lett.* 58, 312–315. doi: 10.1016/S0167-577X(03)00476-2

Zeng, Q., Yu, F., and Dong, G. (2013). Superlubricity behaviors of $Si_3N_4$/DLC Films under PAO oil with nano boron nitride additive lubrication. *Surf. Interface Anal.* 45, 1283–1290. doi: 10.1002/sia.5269

Zhang, D., Li, S., Zuo, X., Guo, P., Ke, P., and Wang, A. (2020). Structural and mechanism study on enhanced thermal stability of hydrogenated diamond-like carbon films doped with Si/O. *Diam. Relat. Mater.* 108:107923. doi: 10.1016/j.diamond.2020.107923

Zhao, F., Bai, Z., Fu, Y., Zhao, D., and Yan, C. (2012). Tribological properties of serpentine, $La(OH)_3$ and their composite particles as lubricant additives. *Wear* 288, 72–77. doi: 10.1016/j.wear.2012.02.009

**Conflict of Interest:** The authors declare that the research was conducted in the absence of any commercial or financial relationships that could be construed as a potential conflict of interest.

*Copyright © 2021 Gao, Wang, Shirani, Chang and Berman. This is an open-access article distributed under the terms of the Creative Commons Attribution License (CC BY). The use, distribution or reproduction in other forums is permitted, provided the original author(s) and the copyright owner(s) are credited and that the original publication in this journal is cited, in accordance with accepted academic practice. No use, distribution or reproduction is permitted which does not comply with these terms.*